

Crystalline water ice on the Kuiper belt object (50000) Quaoar

David C. Jewitt¹ & Jane Luu²

¹Institute for Astronomy, 2680 Woodlawn Drive, Honolulu, Hawaii 96822, USA
²MIT Lincoln Laboratory, Lexington, Massachusetts 02420, USA

The Kuiper belt is a disk-like structure consisting of solid bodies orbiting the Sun beyond Neptune¹. It is the source of the short-period comets and the likely repository of the Solar System's most primitive materials². Surface temperatures in the belt are low (~50 K), suggesting that ices trapped at formation should have been preserved over the age of the Solar System. Unfortunately, most Kuiper belt objects are too faint for meaningful compositional study, even with the largest available telescopes. Water ice has been reported in a handful of objects^{3–5}, but most appear spectrally featureless^{5,6}. Here we report near-infrared observations of the large Kuiper belt object (50000) Quaoar, which reveal the presence of crystalline water ice and ammonia hydrate. Crystallinity indicates that the ice has been heated to at least

110 K. Both ammonia hydrate and crystalline water ice should be destroyed by energetic particle irradiation on a timescale of about 10⁷ yr. We conclude that Quaoar has been recently resurfaced, either by impact exposure of previously buried (shielded) ices or by cryovolcanic outgassing, or by a combination of these processes.

Object (50000) Quaoar (formerly 2002 LM60) is, after Pluto, the largest and brightest known Kuiper belt object. Its diameter and red geometric albedo are 1,260 ± 190 km and 0.09^{+0.04}_{-0.02}, respectively⁷. Quaoar therefore constitutes a particularly attractive target for spectroscopy in search of exposed volatiles. We observed Quaoar using the CISCO spectrometer⁸ at the Subaru 8-m telescope, on UT 2004 May 8 and 9. Quaoar had heliocentric distance 43.37 AU, geocentric distance 42.46 AU and phase angle 0.58°. The apparent visual magnitude was approximately V = 18.5.

The resulting albedo spectrum is plotted in Fig. 1, including data from three infrared grating settings as well as an optical spectrum⁹, all normalized to a red geometric albedo p_R = 0.09 (ref. 7). Inclusion of the optical spectrum gives continuous wavelength coverage from 0.4 to 2.5 μm. The unsmoothed spectrum is shown in Fig. 1 as a black line. Superimposed as a red line is a lightly smoothed spectrum to guide the eye. Regions of high noise are seen near 1.4, 1.9 and longward of 2.4 μm, corresponding to telluric absorption by atmospheric water vapour.

The most important spectral features in Quaoar include a steep, positively sloped continuum from 0.4 to ~1.3 μm wavelength (Fig. 1). This is characteristic of a strong ultraviolet absorber, probably associated with an organic surface composition¹⁰. Additional absorption bands at 1.5 and 2.0 μm (Fig. 2) indicate water ice, while a band at 1.65 μm is characteristic of crystalline (as opposed to amorphous) structure in the ice¹¹. Spectra of other Kuiper belt objects in which water is detected have lacked the quality needed to show the 1.65-μm band^{3,4,5}. Comparison of the pure-

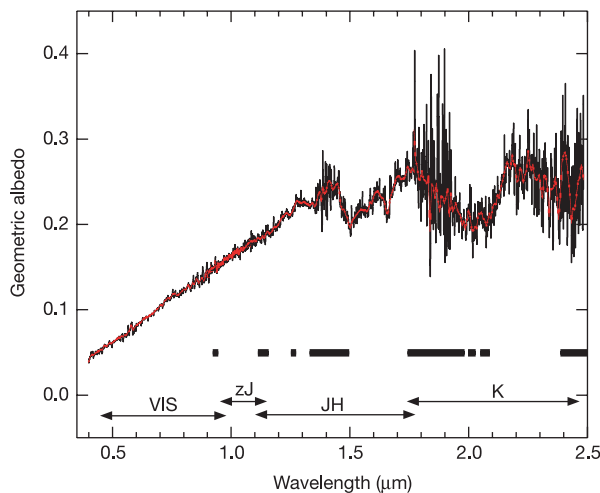


Figure 1 Albedo spectrum of Quaoar showing red optical continuum and distinct absorption bands at 1.5, 1.65 and 2.0 μm. Spectra from four gratings (VIS is from ref. 9, zJ, JH and K are different CISCO grating settings) were spliced together using regions of spectral overlap (see Table 1) and normalized to the R-band geometric albedo of 0.09 at 0.65-μm wavelength⁷. Uncertainty in the levels of the different segments of the spectra is ~5% or less. The black line shows the unsmoothed data. The red line shows a running box-average with a smoothing width of 100 Å in VIS, 40 Å in zJ, 140 Å in JH and 140 Å in K. Wavelengths at which the atmospheric transmission is ≤80% are marked with horizontal bars. CISCO uses a 1,024 × 1,024 pixel HgCdTe 'HAWAII' infrared array as detector with image scale 0.105 arcsec pixel⁻¹, and field width 108 arcsec. Quaoar was acquired by imaging with the grating removed from the spectrograph and confirmed from its proper motion relative to background objects. The spectrograph slit was aligned parallel to the proper motion and the telescope guided at sidereal rates. Seeing on both nights was near 0.4 arcsec at J and 0.3–0.4 arcsec at K, allowing us to use a 0.6-arcsec-wide slit. Individual integration times were 300 s for the zJ and JH spectra, and 250 s for the K spectra: image trail during the integrations was less than 0.2 arcsec. For background subtraction, the spectra were taken in pairs while dithering the image along the slit by 10 arcsec. Approximately every 1.5 h we observed A-type and G-type calibration stars within 0.05 airmasses of Quaoar and, following visits to the stars, we re-centred Quaoar in the slit. Spectra of A-type stars were used to cancel telluric features. Spectra of G-type stars were used to remove the colour of the Sun. The atmosphere was stable with a precipitable water column of ~2 mm. Spectra were flattened, sky-subtracted, traced and extracted using a 1.05-arcsec-wide aperture.

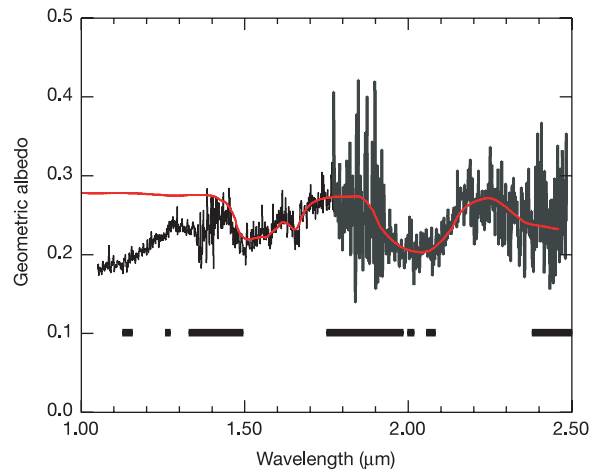


Figure 2 Near-infrared reflection spectrum of Quaoar (black) compared with a water-ice reflection spectrum¹⁰ (red). The water spectrum has not been fitted to the data except for vertical scaling to match the depth of the 2-μm band. Wavelengths at which the atmospheric transmission is ≤80% are marked with horizontal bars. In the 0.4 to 0.95-μm region, the slope normalized to 0.65 μm is S'_{0.65} = 28 ± 2%/1,000 Å (ref. 9). In our zJ spectrum (0.89 to 1.10 μm) the slope normalized in the same way is S'_{0.65} = (27 ± 1)%/1,000 Å, whereas at longer wavelengths the reddened continuum becomes neutral. Broad absorption bands centred near 1.5 and 2.0 μm unambiguously reveal the presence of water ice on Quaoar. A third, weak water-ice band near 1.3 μm (ref. 11) may be evident in the spectrum but is partially overlapped by a telluric feature. The band depths (22% for the 2.0-μm band) and the geometric albedo outside the bands both suggest that the ice is impure, or that ice occupies only a small part of the total surface of (50000) Quaoar. A relatively narrow (0.015 μm) absorption near 1.65 μm is characteristic of cold, crystalline water ice and is specifically not present in pure, amorphous ice^{11,12}.

water-ice spectrum with the data reveals a more subtle feature near 2.2 μm (Fig. 3) which coincides with a band due to ammonia hydrate ($\text{NH}_3 \cdot \text{H}_2\text{O}$)^{12,13}. At 40 K, the 1.5 and 2.0- μm bands have peak absorption coefficients of ~ 50 and $\sim 100 \text{ cm}^{-1}$, respectively¹², corresponding to photon penetration depths in ice of about 0.2 and 0.1 mm. The spectrum therefore samples ice in the very uppermost layers on Quaoar.

A search for other plausible ices was unsuccessful. The spectrum is unlike that of Pluto (compare with Fig. 4), which is dominated by CH_4 and which also shows solid N_2 and CO (ref. 14). Our ability to detect N_2 and CO is questionable, given the spectral resolution of our data, but the eight strong bands of CH_4 in the 1.0 to 2.4 μm spectral region are conspicuously absent in Quaoar, eliminating any possibility that the 1.65- μm feature is methane-contaminated. CO_2 is not present either, down to the level of the noise in the spectrum. Quaoar is spectrally much more similar to Charon, in showing strong water-ice bands and a weak absorption due to ammonia hydrate^{15,16}. The absence of other molecules is unsurprising given the small size and low ($\sim 500 \text{ m s}^{-1}$) escape velocity of Quaoar.

The detection of crystalline ice on Quaoar shows that the temperature has exceeded the critical $T_c \approx 105\text{--}125 \text{ K}$ range for crystallization (see Fig. 1 of ref. 17). The radiation equilibrium temperature (for albedo ~ 0.1 and distance $\sim 43 \text{ AU}$) is only $\sim 50 \text{ K}$. Temperatures higher than T_c could be generated through radioactive decay heating in the interior of Quaoar¹⁸ but not on the surface, where the temperature is limited by radiation to space. Impact heating by micrometeorites could be responsible for heating surface ice above the crystallization temperature. However, the vapour pressures of ammonia and water are very different, and

impact heating is expected to lead to the progressive loss of ammonia from the surface¹⁹. Impact heating thus appears at odds with the presence of ammonia hydrate unless this can be resupplied by another process.

A further complication arises from the instability of crystalline ice and ammonia hydrate to energetic particle bombardment. At low temperatures, crystalline ice is converted to the amorphous phase by the bond-breaking effects of cosmic rays and solar wind particles^{20,21}. Ammonia hydrate is also unstable to energetic particle bombardment, with a survival time of $< 10^6 \text{ yr}$ at Saturn¹⁹. The timescale for complete processing of the optically active top (0.1- μm thick) layer at 40 AU is $\sim 10^7 \text{ yr}$ (ref. 22), much less than the age of the Solar System. Persistence of crystalline ice and ammonia hydrate at the surface therefore implies either that the ice is protected (for example, by a magnetosphere or by an atmosphere, neither of which seems likely at Quaoar) or that the observed ice has been replenished within the past 10^7 yr . On Charon, ammonia hydrate could be chemically produced from a constant supply of nitrogen fed to the surface by the escaping N_2 atmosphere

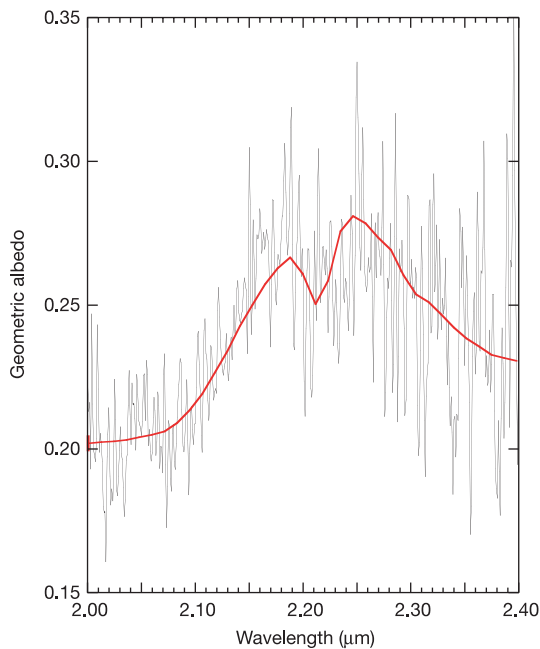


Figure 3 Close-up of the reflection spectrum of Quaoar centred at 2.2 μm . Unsmoothed data are shown by a black line. A model of ammonia hydrate $\text{NH}_3 \cdot \text{H}_2\text{O}$ (3% ammonia)¹⁶ is overplotted in red. Unlike pure water ice, which has a reflection maximum at 2.2 μm (compare with Fig. 2), both Quaoar and ammonia hydrate show a local minimum at this wavelength. The Quaoar band is centred at $2.220 \pm 0.005 \mu\text{m}$ and has a depth of about 10% relative to the local continuum. For comparison, the wavelength of the vibrational overtone of N-H in pure ammonia ice is 2.24 μm , significantly longer than observed, but in ammonia hydrate ($\text{NH}_3 \cdot \text{H}_2\text{O}$) at 65 K the band wavelength is 2.21 μm (refs 12, 13), which overlaps the measured value. The absence of other ammonia hydrate bands (at 1.04, 2.0 and 2.3 μm) in our data is consistent with model spectra provided the fractional amount of NH_3 is $\leq 10\%$ (ref. 16). A similar band has been reported at 2.20–2.22 μm in Pluto's satellite Charon^{15,16} and at 2.21 μm on Uranus' satellite Miranda²³.

Table 1 Parameters of the spectra

Date	Grating	Wavelength*	Spectral dispersion (\AA pixel^{-1})	Integration time (s)
08 May	zJ	0.89–1.30	5.83	1,800
09 May	zJ	0.89–1.30	5.83	1,800
08 May	JH	1.05–1.90	8.23	2,400
09 May	JH	1.05–1.90	8.23	2,400
08 May	HK	1.77–2.49	8.63	6,000
09 May	HK	1.77–2.49	8.63	1,500

*Approximate minimum and maximum wavelengths (in μm) recorded in each spectrum.

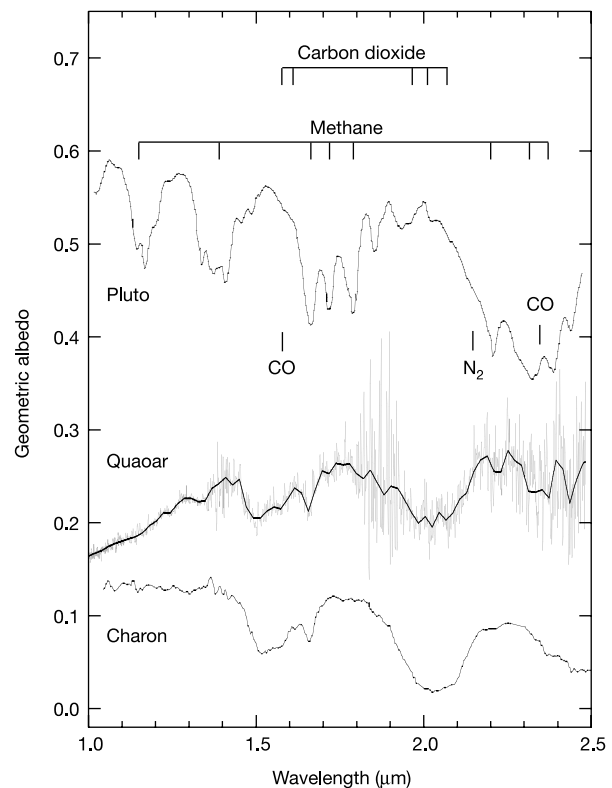


Figure 4 Near-infrared spectra of Pluto, Quaoar and Charon compared. The Pluto and Charon spectra¹⁵ have been displaced vertically and scaled to facilitate comparison with the spectrum of Quaoar. Wavelengths of absorption bands of solid CO , CO_2 , N_2 and CH_4 ice are indicated.

of nearby Pluto¹⁶. There is no corresponding external source of nitrogen at Quaoar (or Miranda²³), and an internal source must be presumed.

Impacts into the surface could mix unirradiated (ammonia-rich, crystalline) subsurface material with the irradiated surface ice. Alternatively, or perhaps in combination with impact ‘gardening’, subsurface material could be exposed by continued outgassing onto the surface as a result of cryovolcanism. Complex geology on small icy satellites, including several smaller than Quaoar, provides pervasive evidence for solid-state convection that could bring warm, ammoniated ice towards the surface²⁴. The energy sources driving this activity are not fully understood, but are likely to include radioactivity and tidal heating (in planet–satellite systems). Ammonia hydrate is an expected product of condensation in the high-density protoplanetary subnebulae, and evidence from the comets, where the ammonia abundance is ~1%, shows that this molecule is also trapped from the solar nebula²⁵. It may play a central role in satellite thermal evolution and geology by decreasing the viscosity and enabling the flow of ice²⁶. Quaoar is certainly large enough to be cryovolcanically active and the crystalline ice and ammonia hydrate are consistent with the products of such activity. □

Received 27 August; accepted 7 October 2004; doi:10.1038/nature03111.

1. Jewitt, D. & Luu, J. Discovery of the candidate Kuiper belt object 1992 QB1. *Nature* **362**, 730–732 (1993).
2. Davies, J. & Barrera, L. (eds) *The First Decadal Review of the Edgeworth–Kuiper Belt* (Kluwer Academic, Dordrecht, 2004).
3. Brown, R. H., Cruikshank, D. P. & Pendleton, Y. Water ice on Kuiper Belt object 1996 TO66. *Astrophys. J. Lett.* **519**, 101–104 (1999).
4. Fornasier, S., Dotto, E., Barucci, M. A. & Barbieri, C. Water ice on the surface of the large TNO 2004 DW. *Astron. Astrophys.* **422**, L43–L46 (2004).
5. Jewitt, D. C. & Luu, J. X. Colors and spectra of Kuiper Belt Objects. *Astron. J.* **122**, 2099–2114 (2001).
6. Licandro, J., Ghinassi, F. & Testi, L. Infrared spectroscopy of the largest known trans-Neptunian object 2001 KX76. *Astron. Astrophys.* **388**, L9–L12 (2002).
7. Brown, M. E. & Trujillo, C. A. Direct measurement of the size of the large Kuiper Belt object (50000) Quaoar. *Astron. J.* **127**, 2413–2417 (2004).
8. Motohara, K. et al. CISCO: Cooled infrared spectrograph and camera for OHS on the Subaru telescope. *Publ. Astron. Soc. Jpn* **54**, 315–325 (2002).
9. Marchi, S., Lazzarin, M., Magrin, S. & Barbieri, C. Visible spectroscopy of the two largest known trans-Neptunian objects: Ixion and Quaoar. *Astron. Astrophys.* **408**, L17–L19 (2003).
10. Cruikshank, D. P. et al. The composition of Centaur 5145 Pholus. *Icarus* **135**, 389–407 (1998).
11. Grundy, W. M. & Schmitt, B. The temperature-dependent near-infrared absorption spectrum of hexagonal H₂O ice. *J. Geophys. Res.* **103**, 25809–25822 (1998).
12. Schmitt, B., Quirico, E., Trotta, F., Grundy, W. M. in *Solar System Ices* (eds Schmitt, B., de Bergh, C. & Festou, M.) 199–240 (Vol. 227, Astrophysics and Space-Science Library, Kluwer Academic, Dordrecht, 1998).
13. Dalton, J. B., Curchin, J. M. & Clark, R. N. Temperature dependence of cryogenic ammonia-water ice mixtures and implications for icy satellite surfaces. *Lunar Planet. Inst. Conf. Abstr.* **32**, 1496 (2001).
14. Owen, T. C. et al. Surface ices and the atmospheric composition of Pluto. *Science* **261**, 745–748 (1993).
15. Brown, M. E. & Calvin, W. M. Evidence for crystalline water and ammonia ices on Pluto’s satellite Charon. *Science* **287**, 107–109 (2000).
16. Dumas, C., Terrile, R. J., Brown, R. H., Schneider, G. & Smith, B. A. Hubble Space Telescope NICMOS spectroscopy of Charon’s leading and trailing hemispheres. *Astron. J.* **121**, 1163–1170 (2001).
17. Jenniskens, P., Blake, D. F., Kouchi, A. in *Solar System Ices* (eds Schmitt, B., de Bergh, C. & Festou, M.) 139–155 (Vol. 227, Astrophysics and Space-Science Library, Kluwer Academic, Dordrecht, 1998).
18. Choi, Y., Cohen, M., Merk, R. & Prrialnik, D. Long-term evolution of objects in the Kuiper Belt zone—Effects of insolation and radiogenic heating. *Icarus* **160**, 300–312 (2002).
19. Lanzerotti, L. J., Brown, W. L., Marcantonio, K. J. & Johnson, R. E. Production of ammonia-depleted surface layers on the saturnian satellites by ion sputtering. *Nature* **312**, 139–140 (1984).
20. Hansen, G. B. & McCord, T. B. Amorphous and crystalline ice on the Galilean satellites: A balance between thermal and radiolytic processes. *J. Geophys. Res.* **109**, CiteID E01012 (2004).
21. Strazzulla, G., Leto, G., Baratta, G. A. & Spinella, F. Ion irradiation experiments relevant to cometary physics. *J. Geophys. Res.* **96**, 17547–17552 (1991).
22. Cooper, J. F., Christian, E. R., Richardson, J. D. & Wang, C. Proton irradiation of Centaur, Kuiper Belt, and Oort Cloud objects at plasma to cosmic ray energy. *Earth Moon Planets* **92**, 261–277 (2003).
23. Bauer, J. M. et al. The near infrared spectrum of Miranda: Evidence of crystalline water ice. *Icarus* **158**, 178–190 (2002).
24. Czechowski, L. & Leliwa-Kopystyński, J. Tidal heating and convection in the medium sized icy satellites. *Celest. Mech. Dyn. Astron.* **87**, 157–169 (2003).
25. Kawakita, H. & Watanabe, J. Revised fluorescence efficiencies of cometary NH₂: Ammonia abundance in comets. *Astrophys. J. Lett.* **572**, 177–180 (2002).
26. Stevenson, D. J. Volcanism and igneous processes in small icy satellites. *Nature* **298**, 142–144 (1982).

Acknowledgements This paper is based on observations at the Subaru Telescope, which is operated by the National Astronomical Observatory of Japan. We thank K. Aoki and B. Potter for help with CISCO/Subaru and C. Dumas, Y. Fernandez and T. Owen for helpful comments. This work was supported in part by a grant to D.C.J. from NASA.

Competing interests statement The authors declare that they have no competing financial interests.

Correspondence and requests for materials should be addressed to D.C.J. (jewitt@hawaii.edu).

Routing of anisotropic spatial solitons and modulational instability in liquid crystals

Marco Peccianti¹, Claudio Conti¹, Gaetano Assanto¹, Antonio De Luca² & Cesare Umetsu²

¹NooEL (Nonlinear Optics and Optoelectronics Laboratory), National Institute for the Physics of Matter (INFN) and Department of Electronic Engineering, University “Roma Tre”, Via della Vasca Navale, 84, 00146 Rome, Italy

²LICRYL (Liquid Crystals Laboratory), National Institute for the Physics of Matter (INFN), Center of Excellence CEMIF.CAL and Department of Physics, University of Calabria, 87036 Arcavacata di Rende (CS), Italy

In certain materials, the spontaneous spreading of a laser beam (owing to diffraction) can be compensated for by the interplay of optical intensity and material nonlinearity. The resulting non-diffracting beams are called ‘spatial solitons’ (refs 1–3), and they have been observed in various bulk media^{4–6}. In nematic liquid crystals^{7–9}, solitons can be produced at milliwatt power levels^{10–12} and have been investigated for both practical applications¹³ and as a means of exploring fundamental aspects of light interactions with soft matter^{14,15}. Spatial solitons effectively operate as waveguides, and so can be considered as a means of channelling optical information along the self-sustaining filament. But actual steering of these solitons within the medium has proved more problematic, being limited to tilts of just a fraction of a degree^{16–20}. Here we report the results of an experimental and theoretical investigation of voltage-controlled ‘walk-off’ and steering of self-localized light in nematic liquid crystals. We find not only that the propagation direction of individual spatial solitons can be tuned by several degrees, but also that an array of direction-tunable solitons can be generated by modulation instability^{21–25}. Such control capabilities might find application in reconfigurable optical interconnects, optical tweezers and optical surgical techniques.

Previously investigated angular steering of spatial solitons (SSs) has been limited to very small angles, typically fractions of a degree^{16–20}. There are two reasons for this, one applying to theoretical models, and the other to material systems. First, there is an intrinsic limitation associated with the frequently invoked paraxial approximation. The latter allows the understanding of most SS physics, but its validity is limited to wavepackets localized on-axis with respect to the source light beam. Large-angle steering is ruled out by such treatment, if used in a consistent way. Second, the most studied SSs in bulk matter (such as 2D + 1 parametric and photorefractive solitons^{26,27}) require propagation in anisotropic crystals; in actual arrangements, such material complexity places severe constraints (for example, phase-matching in parametric SSs and anisotropic charge drift/diffusion in photorefractive SSs) on the experimental observation of SSs with adjustable directions of propagation. Hence, a number of simplifying assumptions have